Available online at www.sciencedirect.com

ScienceDirect

IFAC Papers Online CONFERENCE PAPER ARCHIVE

IFAC PapersOnLine 51-34 (2019) 28–33

A Robust Iterative Learning Switching Controller for following Virtual Constraints: Application to a Hybrid Neuroprosthesis

Vahidreza Molazadeh, Zhiyu Sheng, Xuefeng Bao, and Nitin Sharma

***Abstract*—In this paper, a robust iterative learning switching controller that uses optimal virtual constraint is designed for a hybrid walking exoskeleton that uses functional electrical stimulation and a powered exoskeleton. The synthesis of iterative learning control with sliding-mode control improves tracking performance and accuracy. The motivation for designing this switching controller was to obtain joint torques either from functional electrical stimulation or electric motor. A generalized switching controller is utilized to switch based on the stimulated muscle fatigue state. For achieving stability in walking cycle, the controller is used to force the system to follow the designed virtual constraints. The combination of sequential quadratic programming and genetic-particle swarm optimization algorithm is used for deriving the virtual constraints. The effectiveness of the new iterative learning control for output tracking is verified in a simple model of walking (3-link) that has active actuation at the hip joints.**

Introduction

Functional electrical stimulation (FES) and powered exoskeletons are two viable technologies that have the potential to restore walking ability in persons with spinal cord injuries [1]–[3]. FES artificially excites paralyzed muscles through external electrical current and has been successfully shown to reproduce walking movement. However, FES is susceptible to fatigue, which results loss of muscle excitability and its subsequent use. Unlike FES, powered exoskeletons can reliably produce torque but they may be heavy and bulky to wear. The combination of FES and powered exoskeletons may overcome these limitations. For example, a hybrid device, composed of electrical motors and FES, may need smaller motors because the electric muscle stimulation can share work load. This can conceivably improve wear-ability. The hybrid device can also improve torque reliability during muscle fatigue by allocating more control effort to electric motors. This can conceivably help in achieving a longer walking duration with the device. Furthermore, the exoskeletal frame can constrains any unwanted degrees of freedom and decrease FES stimulation duty cycle. Moreover, the use of the hybrid also gains from the therapeutic benefits of FES such as, preventing muscle atrophy.

However, there is a limited research on control algorithms and gait design of a hybrid neuroprosthesis due to the challenges faced in the control design of these systems. One of the challenges is that both the FES and motor can act at a limb joint, which induces input redundancy. In [4], an adaptive control allocation method was used to allocate a portion of control to the electric motors and the rest of that to the FES. In both [1] and [2], the motors were controlled based on the joint angles and the FES was controlled by combining the PID and iterative learning control methods. Authors in [5] develop a model based control allocation for a hybrid neuroprosthesis, which incorporates FES with an electric motor to share the work load for alleviating effects of FES-induced fatigue of muscle. An NMPC-based DCA method determine the control effort allocation that use a gradient projection-based optimization technique.

Aforementioned works focused on shared control strategy; i.e., both FES and powered exoskeleton simultaneously provide inputs. An alternative strategy to control the hybrid neuroprosthesis employs a switching controller, which switches between FES and an electric motor based on the reduced or recovered control effectiveness of the user's muscle force output. By using this method, the user's muscles are allowed to recover from muscle fatigue by making the electric motors mainly responsible for the limb joints movement. Whenever muscles recover, FES can be mainly used again to produce limb movements.

Another major challenge for using hybrid exoskeletons is that by far, the most common method for gait design of such systems is the tracking of precomputed desired trajectory such as in [6]–[8]. Trajectory design and tracking multiple joints are challenging. Instead of using time dependent trajectories, movement of the lower-limb joints can be designed with either passive constraints imposed by the geometric constraints of the exoskeleton, or by using virtual constraints imposed by actuators [9], [10]. Virtual constraints have superiority over passive constraints because they give the user and the system more freedom and stability, and let the system behave more efficiently [11], [12].

This paper extends the switching control design in [13] to a multi-DOF walking, adds a learning procedure, and instead of tracking time-based joint angle trajectories, the lower-limb

Vahidreza Molazadeh, Zhiyu Sheng, Xuefeng Bao and Nitin Sharma are with the Department of Mechanical Engineering and Materials Science, University of Pittsburgh, Pittsburgh, PA,USA 15261. Nitin Sharma is also with the Department of Bioengineering at the University of Pittsburgh. Email:{vam50, zhs41, XUB3, nis62}@pitt.edu. This work was funded in part by National Science Foundation award number 1646009. Any opinions, findings, and conclusions or recommendations expressed in this material are those of the author(s) and do not necessarily reflect the views of the National Science Foundation.

10.1016/j.ifacol.2019.01.011

joints movement is self-generated via a time-invariant manifold which is based on virtual constraints concept [9], [14], [15]. In fact, in this paper, we utilize virtual constraints for the hybrid exoskeletons to design a unified (virtual constraint + switching + iterative leaning) optimal, and robust controller. In our previous work [16], we used feedback linearization method for controlling the system which has considerable downside due to the requirement of exact model knowledge (EMK). Therefore, in this paper an iterative learning term is used to estimate system dynamics. The stability of the controller is proved for this new switching+learning controller. The switching controller, in this paper, switches between an electric motor and FES based on effectiveness of user's muscle force output. There are several challenges for using this type of switching+learning controller. One of the most important problems is to prove stability despite arbitrarily switching between the FES and the electric motor. Another problem is the considerable uncertainties in musculoskeletal dynamics, which forces the controller to be robust enough against the uncertainties during practical implementation.

To address these problems, an iterative learning switching integral sliding mode control technique, which is robust to uncertainties of the system, is implemented on a generalized hybrid neuroprosthesis and the system stability is also proven. A more generalized switched cases family are considered in the design that do switching based on the normalized muscle fatigue variable. By utilizing the combination of sequential quadratic programming (SQP) method and genetic-particle swarm optimization algorithm (GAPSO), the virtual constraints are obtained. GAPSO is used for achieving an acceptable semi-optimal manifold for system virtual constraints. Then, the results are utilized as a starting point for the SQP in order to find an optimal solution without needing to a high sampling rate and evolution cycles for GAPSO. Therefore, with this procedure, the optimal solution that satisfies all the constraints can be obtained, and meanwhile, the virtual constraints can be re-planned in semi-real-time, which lets the system to redesign the virtual constraints after few steps if required.

I. General Walking Model Equation with Impact Effects

The complete model of walking, N-DOF which includes impulse effects of ground impact, in the state space form, can be written as,

$$\begin{cases} \dot{x} = f(x) + g(x)T & x^-(t) \notin S \\ x^+ = \triangle(x^-) & x^-(t) \in S \end{cases} \tag{1}$$

where x =$[q, \dot{q}]^T$, $q \in \mathbb{R}^N$ is defined as $q = [\theta_1 \theta_2 \cdots \theta_N]$. ω_i and θ_i are the i-th linkage angular velocity and deflection angle, respectively. $S = \left\{(\theta, \omega) \in \chi \mid \theta_i = \theta_i^d\right\}$, θ_i^d is the final value of θ_i in a step, which is a criterion which shows that a step is completed, $f(x)$ is the compact form of $\begin{bmatrix} \begin{bmatrix} \emptyset_{N\times N} & I_{N\times N} \end{bmatrix}^T & \cdots \\ \cdots & \left[D(q)^{-1}(-C(q,\dot{q})\dot{q} - G(q) + \tau_p)\right]^T \end{bmatrix}^T$ and $g(x)$ is the compact form of $\begin{bmatrix} 0 & 0 \cdots & 0 & \left[D(q)^{-1}(B(q)T)\right]^T \end{bmatrix}^T$, where $B \in \mathbb{R}^{N\times N-1}$ is a control gain matrix, $C \in \mathbb{R}^{N\times N}$ is a Centripetal-Coriolis matrix, $D \in \mathbb{R}^{N\times N}$ is an inertia matrix, $G \in \mathbb{R}^N$ is a gravity vector, $T \in \mathbb{R}^{N-1}$is the input torque and $\tau_p(q, \dot{q}) \in \mathbb{R}^N$ is the passive joint moment in the musculoskeletal dynamics. The i-th link moment is defined as

$$\tau_{p_i} = d_{1_i}(\vartheta_i - \vartheta_{0_i}) + d_{2_i}\dot{\vartheta}_i + d_{3_i}e^{d_{4_i}\vartheta_i} - d_{5_i}e^{d_{6_i}\vartheta_i} \tag{2}$$

where ϑ_i is the joint anatomical angle which is the angle between the position of the interest and a segment's anatomical position, of the i-th linkage, and $\vartheta_{0_i}$and d_{j_i} are positive constants. The double support phase is assumed as instantaneous moment that includes impulsive effect of ground impact, the impact model of [17] is implemented under the assumption that the stance leg end is not slipping and it is in contact with the ground surface [18]. Using the angular momentum conservation law, the post impact state values, $x^+ = (q^+, \omega^+)$ can be obtained by a function $\triangle \in \mathbb{R}^{2N\times 1}$ with the values of state before impact, $x^- = (q^-, \omega^-)$.

A. Joint Actuation

An electrical stimulation for the extensor muscles, an electrical stimulation for the flexor muscles, and an electric motor, actuate each linkage. The joint torque, $T_i\,(i = 1,\, 2,\, N)$, can be defined as

$$T_i = T_{ag_i} - T_{ant_i} + T_{m_i} \tag{3}$$

where $T_{ant_i}$and T_{ag_i} are the torques produced by antagonist muscles and the electrical stimulation of the agonist muscles and, respectively and T_{motor} is the electrical motor torque. The torque of the motor at the i-th link is given as

$$T_{m_i} = k_{m_i}u_{m_i}. \tag{4}$$

In (4) $u_{m_i} \in \mathbb{R}$ is the current amplitude to the electric motor and $k_{m_i} \in \mathbb{R}$ is the torque constant of electric motor. The torque produced by electrical stimulation of antagonist and agonist muscles is obtained by

$$T_{ag/ant} = \psi_{l_i}(\vartheta_i)\psi_{v_i}(\omega_i)\mu_i u_i. \tag{5}$$

In (5), $\mu_i \in \mathbb{R}$ is the normalized fatigue variable, $u_i \in \mathbb{R}$ is the normalized muscle stimulation, and $\psi_{l_i}(\vartheta) \in \mathbb{R}^+$and $\psi_{\nu_i}(\dot{\vartheta}) \in \mathbb{R}^+$are the torque-length and torque-velocity relationships of the flexor/extensor muscles, respectively. As in [19], the equations of torque-length and torque-velocity, for i-th link, can be defined as

$$\psi_{l_i}(\vartheta_i) = c_{1_i}e^{\frac{-\left(\vartheta_i - c_{2_i}\right)^2}{2c_{3_i}}} \tag{6}$$

$$\psi_{v_i}(\omega_i) = c_{4_i}\left[1 + tanh\left(c_{5_i}\omega_i + \frac{1}{c_{4_i}}\right)\right]. \tag{7}$$

The parameters c_{1_i}, c_{3_i}, c_{4_i} and c_{5_i} should be positive for guaranteeing that $\psi_{l_i}(\vartheta)\psi_{v_i}(\omega_i) > 0$ and $c_{2_i} \geqslant 0$. The reason for constraining these parameters is that the muscles can only produce a positive contractile force. Based on [20], the following differential equation is used for deriving the normalized muscle fatigue, μ_i, in (5)

$$\dot{\mu}_i = \frac{1}{t_{f_i}}\left(\mu_{min_i} - \mu_i\right)u_{h_i} + \frac{1}{t_{r_i}}\left(1 - \mu_i\right)\left(1 - u_{h_i}\right) \tag{8}$$

where, $\mu_{min_i} \in (0,\,1]$ is the fatigue constant and $t_{f_i}, t_{r_i} \in \mathbb{R}^+$ are time constants for fatigue and fatigue recovery in the muscle, respectively.

B. Switched System

The system with switching can be expresses as

$$\begin{aligned} &D(q)\ddot{q} + C(q,\dot{q}).\dot{q} + G(q) + \tau_p \\ &= B(q)\left(a_n\iota_n T - (I_{N-1\times N-1} - a_n)\iota_n T + \varsigma_n T\right) \end{aligned} \tag{9}$$

where $T = a_n\iota_n T - (I_{N-1\times N-1} - a_n)\iota_n T + \varsigma_n T =$, $T_{ant} = a_n\iota_n T = T_{ag}$, $-(I_{N-1\times N-1} - a_n)\iota_n T$, $T_m = \varsigma_n T$, and $\iota_n, \varsigma_n \in R^{+^{N-1\times N-1}}$ belongs to the finite set of switch family,

$$\begin{aligned} &\Omega = \\ &\{(\iota_1,\varsigma_1,a_1),(\iota_2,\varsigma_2,a_2),\ldots,(\iota_{N_\Omega},\varsigma_{N_\Omega},a_{N_\Omega})\cdots \\ &\cdots \left| a_n = diag(\ a_{n_1}\quad a_{n_2}\quad \cdots\quad a_{n_{N-1}}\ ),\cdots \right. \\ &\cdots \iota + \varsigma_n = I_{N-1\times N-1},\ a_{n_i} \in \{0,1\},\ n = 1,2,\ldots,N_\Omega\} \end{aligned} \tag{10}$$

where N_Ω is the number of combinations. (ι_n, ς_n) are chosen based on the variable of muscle fatigue, μ.

Remark 1. Note that based on the type of muscle being recruited (i.e., flexor or extensor), a_{n_i} can be either 0 or 1.

II. Virtual Constraint and Controller Design

A. Virtual Constraint Design

Based on [14], the output, $y \in \mathbb{R}^{N-1}$, can be defined as

$$y = h_0(q) – h_d(\theta(q)). \tag{11}$$

The system has one degree of underactuation for torso. Therefore, the size of y is $N-1$. In (11), $h_0(q)$ is a function of the independent joint angles which based on the current arrangement of the output is obliged to follow $h_d(\theta(q))$, which is a desired virtual constraint function that can be expressed with the Bezier polynomials as

$$h_d\left(\theta(q)\right) = \begin{bmatrix} b_1\left(w(q)\right) \\ b_2\left(w(q)\right) \\ \vdots \\ b_{N-1}\left(w(q)\right) \end{bmatrix} \tag{12}$$

where

$$b_i(w) = \sum_{k=0}^{M} \varrho_k^i \frac{M!}{k!(M-k)!} w^k (1-w)^{M-k}. \tag{13}$$

In (13) M is an integer that shows the number of Bezier polynomial terms, ϱ_k^i is the optimization parameter, and w is obtained according to the following equation.

$$w(q) = \frac{\theta(q) - \theta^+}{\theta^- - \theta^+}. \tag{14}$$

In (14), $\theta^-$and $\theta^+$are minimum and maximum value of the $\theta(q)$ respectively. $\theta(q)$ is a function of joints angles and is defined as $\theta(q) = \zeta_1\theta_1 + \zeta_2\theta_2 + \ldots + \zeta_n\theta_N$. $\zeta_i \in \mathbb{R}$ are chosen such that $\theta(q)$ is increasing monotonically.

B. Controller Design

The the controller goal is to make the output zero or in other words, force $h_0(q)$ to follow $h_d(q)$. Therefore, the output should be expressed as follow (15).

$$y = h(q) \tag{15}$$

and thus

$$\frac{d^2y}{dt^2} = L_f^2 h(q,\dot{q}) + L_g L_f h(q) T \tag{16}$$

where $L_g L_f h$ is the decoupling matrix. The invertibility of this matrix at a point guarantees the zero dynamics uniqueness and existence in the neighborhood of that point [21]. For each output y_i, $(i = 1\ldots N-1)$, if it is considered that $\bar{y}_{1,i} = y_i$ and $\bar{y}_{2,i} = \dot{y}_i$, (16) can be rewritten as

$$\begin{aligned} \dot{\bar{y}}_{1,i} &= \bar{y}_{2,i} \\ \dot{\bar{y}}_{2,i} &= \sigma_i^T v_{f,i} + v_{f_2,i} + v_{g,i} T_i + v_{d,i} \end{aligned} \tag{17}$$

where $\sigma_i^T v_{f,i} + v_{f_2,i}$ and $v_{g,i}$ are the $i\,th$ row from $L_{\hat{f}}^2 h(q,\dot{q})$ and $L_{\hat{g}} L_{\hat{f}} h(q)$ respectively, where $\hat{f}$ and $\hat{g}$ are the dynamics nominal models in (1), $\sigma_i^T v_{f,i}$ is linearly parameterizable terms part of the system, $v_{f_2,i}$ is not linearly parameterizable terms and $\sigma_i^T$is unknown time variant function which is learned by iterative learning method and $v_{d,i}$ is the system and input disturbance term due to model uncertainty. For the system stabilization in (17), based on the virtual input, T_i, a controller is designed, so that the pair of allocation coefficient $(\iota_n$,$\varsigma_n)$ can be switched arbitrarily without affecting the stability property of the system. In the next part, an iterative learning continuous integral sliding mode (ILCISM) control technique is implemented and the robust stability is proved.

1) Implementation of ILCISM: For $i = 1\ldots N-1$, let the sliding surface $s_i \in \mathbb{R}$ be defined as $s_i = \lambda_1 e\left(t\right) + \lambda_2 \dot{e}\left(t\right)$, where $e = (\bar{y}_{i,d} - \bar{y}_i)$, $\lambda_i \in \mathbb{R}$ is a constant number, $\bar{y}_{i,d}$ and $\bar{y}_i$ are the desired and the system output respectively such that the system in (17) would equivalently become

$$\dot{s}_{\mathrm{k,i}} = \sum_{j=1}^{2} \lambda_j \bar{y}_{j,d} - \lambda_1 \bar{y}_{1,i} - \sigma_{k,i}^T v_{f,i} - v_{g,i} T_i - v_{f_2,i} - v_{d,i}. \tag{18}$$

Using the subsequent stability analysis and ILCISM [22],

$$\begin{aligned} T_{k,i} = v_{g,i}^{-1} \Bigg(&\sum_{j=1}^{2} \lambda_j \bar{y}_{j,d} - \lambda_1 \bar{y}_{1,i} - \hat{\sigma}_{k,i}^T v_{f,i} - v_{k,i} - v_{f_2,i} \\ &+ \alpha_{1,i} \left|s_{k,i}\right|^{\frac{2}{3}} sgn(s_{k,i}) + \tfrac{4}{3}\alpha_{2,i} sgn(s_{k,i}) + \alpha_{3,i} s_{k,i} \Bigg) \end{aligned} \tag{19}$$

where $i = 1\ldots N-1$, k is the number of iterations, and $\alpha_{1,i}$, $\alpha_{1,i}$ and $\alpha_{3,i}$ are positive constants. $\hat{\sigma}_{k,i}$ is the recursive part of the control. It is used for learning the unknown term $\sigma_{k,i}$, and based on the next section stability analysis, it can be derived using the following update law,

$$\hat{\sigma}_{k,i} = \hat{\sigma}_{k-1,i} - q\xi \left(\frac{4\eta}{3} \left|s_{k,i}\right|^{\frac{1}{3}} sgn\left(s_{k,i}\right) + \gamma s_{k,i} \right) \tag{20}$$

where q, η and γ are constants belonged to $\mathbb{R}^+$. The variable $v_{k,i}$ in (12) is an integral term that is defined as below,

$$\dot{v}_{k,i} = -\beta_1 s_{k,i} - \beta_2 \left|s_{k,i}\right|^{\frac{1}{3}} sgn\left(s_{k,i}\right) \tag{21}$$

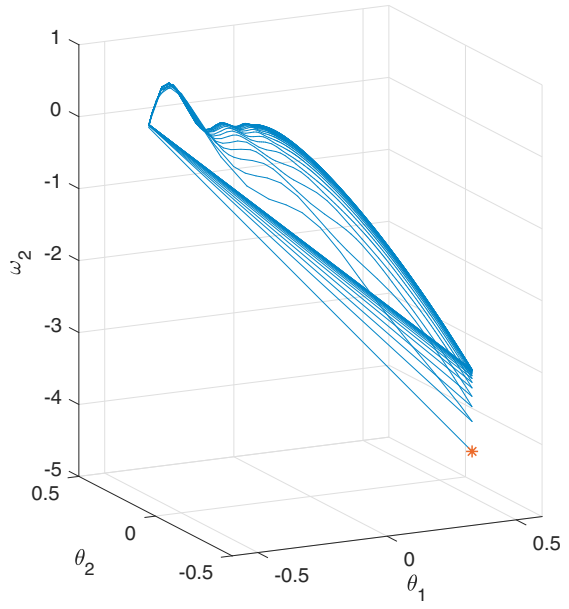

Fig. 1. 3-D diagram, showing attractive limit cycle of the system

where both β_1 and β_2 are positive constants. By using the ILC law (19), the sliding surface dynamic equation can be rewritten as follow,A two-step optimization method and virtual-constraint based switching iterative learning sliding mode control technique has been developed in this paper. According to the simulated results, this technique helps the

$$\begin{aligned}\dot{s}_{k,i} = -\alpha_{3,i}s_{k,i} + \Psi_{k,i}^T v_{f,i} + v_{k,i} - v_{d,k,i} \\ -\alpha_{1,i}\left|s_{k,i}\right|^{\frac{2}{3}} sgn(s_{k,i}) - \tfrac{4}{3}\alpha_{2,i} sgn(s_{k,i})\end{aligned} \tag{22}$$

where $\Psi_{k,i} = \hat{\sigma}_{k,i} - \sigma_{k,i}$.

2) Stability Analysis the Finite Time Convergence: In order to show the stability of the hybrid system that includes the ground impact phase, the system Poincare map is shown in Fig. 1. As, it can bee seen from the figure the gait cycle converges to the limit cycle which was designed by the optimization method in the previous step. According to the figure, the error of the system is reducing after each single ground impact in the compare of previous ground impact. For proving the stability of the learning controller, the following energy function is defined.

$$V_{k,i} = V_{k,i}^{(1)} + V_{k,i}^{(2)} + V_{k,i}^{(3)} + V_{k,i}^{(4)} \tag{23}$$

where $V_{k,i}^{(1)} = \frac{v_{k,i}v_{k,i}}{2}$, $V_{k,i}^{(2)} = \eta\left|s_{k,i}\right|^{\frac{4}{3}}$, $V_{k,i}^{(3)} = \gamma\frac{s_{k,i}s_{k,i}}{2}$, and $V_{k,i}^{(4)} = \frac{1}{2q}\int_{t_{0,k}}^{t}\Psi_{k,i}^T(\tau)\,\Psi_{k,i}(\tau)\,d\tau$. $t_{0,k}$ is the start time of k-th iteration. The convergence of the tracking error will be evaluated based on the difference between energy function between two iterations in a row according to the follow,

$$\Delta V_{k,i}^{(1)} = V_{k,i}^{(1)} - V_{k-1,i}^{(1)} \tag{24}$$

Therefore, using (16),

$$\begin{aligned}\Delta V_{k,i}^{(1)} = -\tfrac{v_{k-1,i}v_{k-1,i}}{2} - \beta_1\int_{t_{0,k}}^{t} v_{k,i}s_{k,i}d\tau \\ -\beta_2\int_{t_{0,k}}^{t} v_{k,i}\left|s_{k,i}\right|^{\frac{1}{3}} sgn\left(s_{k,i}\right)d\tau + C_1.\end{aligned} \tag{25}$$

In a similar way, the difference of k-th and (k-1)-th iteration of the second energy function is obtained,

$$\Delta V_{k,i}^{(2)} = \eta\left|s_{k,i}\right|^{\frac{4}{3}} - \eta\left|s_{k-1,i}\right|^{\frac{4}{3}}, \tag{26}$$

Using the derivative of $\left|s_{k,i}\right|^{\frac{4}{3}}$, the above equation can be written in the following alternative way,

$$\Delta V_{k,i}^{(2)} = \frac{4}{3}\eta\int_{t_{0,k}}^{t}\left|s_{k,i}\right|^{\frac{1}{3}} sgn\left(s_{k,i}\right)\dot{s}_{k,i}d\tau + C_2 - \eta\left|s_{k-1,i}\right|^{\frac{4}{3}}. \tag{27}$$

By substituting (22) into (27), new form of (27) is obtained as,

$$\begin{aligned}\Delta V_{k,i}^{(2)} = +\tfrac{4\eta}{3}\int_{t_{0,k}}^{t}\left|s_{k,i}\right|^{\frac{1}{3}} sgn\left(s_{k,i}\right)v_{k,i}d\tau \\ \tfrac{-4\alpha_3\eta}{3}\int_{t_{0,k}}^{t}\left|s_{k,i}\right|^{\frac{4}{3}}d\tau + \tfrac{4\eta}{3}\int_{t_{0,k}}^{t}\left|s_{k,i}\right|^{\frac{1}{3}} sgn\left(s_{k,i}\right)\Psi_{k,i}^T v_{f,i}d\tau \\ -\tfrac{4\eta}{3}\int_{t_{0,k}}^{t}\left|s_{k,i}\right|^{\frac{1}{3}} sgn\left(s_{k,i}\right)v_{d,i}d\tau - \tfrac{4\alpha_1\eta}{3}\int_{t_{0,k}}^{t}\left|s_{k,i}\right|d\tau \\ -\eta\left|s_{k-1,i}\right|^{\frac{4}{3}} - \tfrac{16}{9}\eta\alpha_{2,i}\int_{t_{0,k}}^{t}\left|s_{k,i}\right|^{\frac{1}{3}}d\tau + C_2\end{aligned} \tag{28}$$

If we consider $\left|v_{d,i}\right| \leq b_d$, where$b_d$ is the upper bound of disturbance of the system, (28) can be rewritten as

$$\begin{aligned}\Delta V_{k,i}^{(2)} \leq \tfrac{-4\alpha_3\eta}{3}\int_{t_{0,k}}^{t}\left|s_{k,i}\right|^{\frac{4}{3}}d\tau - \tfrac{16}{9}\eta\alpha_{2,i}\int_{t_{0,k}}^{t}\left|s_{k,i}\right|^{\frac{1}{3}}d\tau \\ +\tfrac{4\eta}{3}\int_{t_{0,k}}^{t}\left|s_{k,i}\right|^{\frac{1}{3}} sgn\left(s_{k,i}\right)\Psi_{k,i}^T v_{f,i}d\tau - \tfrac{4\alpha_1\eta}{3}\int_{t_{0,k}}^{t}\left|s_{k,i}\right|d\tau \\ -\eta\left|s_{k-1,i}\right|^{\frac{4}{3}} + \tfrac{4b_d\eta}{3}\int_{t_{0,k}}^{t}\left|s_{k,i}\right|^{\frac{1}{3}}d\tau \\ +\tfrac{4\eta}{3}\int_{t_{0,k}}^{t}\left|s_{k,i}\right|^{\frac{1}{3}} sgn\left(s_{k,i}\right)v_{k,i}d\tau + C_2.\end{aligned} \tag{29}$$

The difference of k-th and (k-1)-th iteration of the third energy function is obtained as,

$$\begin{aligned}\Delta V_{k,i}^{(3)} = \gamma\tfrac{s_{k,i}s_{k,i}}{2} - \gamma\tfrac{s_{k-1,i}s_{k-1,i}}{2} \\ = \gamma\int_{t_{0,k}}^{t} s_{k,i}\dot{s}_{k,i}d\tau + C_3 - \gamma\tfrac{s_{k-1,i}s_{k-1,i}}{2}\end{aligned} \tag{30}$$

By substituting (22) into (30) and considering the upper bound, b_d for the uncertainties, the following is achieved.

$$\begin{aligned}\Delta V_{k,i}^{(3)} = -\gamma\tfrac{s_{k-1,i}s_{k-1,i}}{2} - \gamma\alpha_3\int_{t_{0,k}}^{t} s_{k,i}s_{k,i}d\tau \\ +\gamma\int_{t_{0,k}}^{t} s_{k,i}\Psi_{k,i}^T v_{f,i}d\tau - \tfrac{4}{3}\alpha_{2,i}\gamma\int_{t_{0,k}}^{t}\left|s_{k,i}\right|d\tau + C_3 \\ +\gamma\int_{t_{0,k}}^{t} s_{k,i}v_{k,i}d\tau + b_d\gamma\int_{t_{0,k}}^{t}\left|s_{k,i}\right|d\tau - \gamma\alpha_1\int_{t_{0,k}}^{t}\left|s_{k,i}\right|^{\frac{5}{3}}d\tau.\end{aligned} \tag{31}$$

Difference of the last energy function between two iteration in a row can be written as,

$$\Delta V_{k,i}^{(4)} = \frac{1}{2b_q} \int_{t_{0,k}}^{t} \Psi_{k,i}^T \Psi_{k,i} d\tau - \frac{1}{2b_q} \int_{t_{0,k}}^{t} \Psi_{k-1,i}^T \Psi_{k-1,i} d\tau \tag{32}$$

where $b_q \in \mathbb{R}^+$. Based on (20) and [23], the following equation can be derived.

$$\begin{aligned} &\frac{1}{2b_q}\left(\Psi_{k,i}^T \Psi_{k,i} - \Psi_{k-1,i}^T \Psi_{k-1,i}\right) \\ &= \frac{1}{b_q}\left(\hat{\sigma}_{k,i} - \sigma_i\right)^T \left(\hat{\sigma}_{k,i} - \hat{\sigma}_{k-1,i}\right) \\ &-\frac{1}{2b_q}\left(\hat{\sigma}_{k,i} - \hat{\sigma}_{k-1}\right)^T \left(\hat{\sigma}_{k,i} - \hat{\sigma}_{k-1,i}\right). \end{aligned} \tag{33}$$

Based on (20), (33) can be rearranged as,

$$\begin{aligned} &\frac{1}{2b_q}\left(\Psi_{k,i}^T \Phi_{k,i} - \Psi_{k-1,i}^T \Psi_{k-1,i}\right) = \\ &\frac{-4\eta}{3}\left|s_{k,i}\right|^{\frac{1}{3}} sgn(s_{k,i}) \Psi_{k,i} v_{f,i} - \gamma s_{k,i} \Psi_{k,i}^T v_{f,i} \\ &-\frac{1}{2b_q}\left(\hat{\sigma}_{k,i} - \hat{\sigma}_{k-1}\right)^T \left(\hat{\sigma}_{k,i} - \hat{\sigma}_{k-1,i}\right) \end{aligned} \tag{34}$$

(32) can be related to the sliding mode surface as follow,

$$\begin{aligned} &\Delta V_{k,i}^{(4)} = -\frac{1}{2b_q} \int_{t_{0,k}}^{t} \left(\hat{\sigma}_{k,i} - \hat{\sigma}_{k-1}\right)^T \left(\hat{\sigma}_{k,i} - \hat{\sigma}_{k-1,i}\right) d\tau \\ &-\gamma \int_{t_{0,k}}^{t} \left(s_{k,i} \Psi_{k,i}^T v_{f,i}\right) d\tau \frac{-4\eta}{3}\left|s_{k,i}\right|^{\frac{1}{3}} sgn\left(s_{k,i}\right) \Psi_{k,i} v_{f,i} d\tau. \end{aligned} \tag{35}$$

For proving the convergence of both the output tracking error and sliding surface dynamics, we now combine the difference of energy terms for two iterations as below, based on considering $\beta_1 = \gamma$, $\beta_2 = \frac{4\eta}{3}$, $\alpha_{2,i} = \frac{\alpha_1 \eta}{\gamma}$, $\gamma = \frac{4\alpha_1 \eta}{3b_d}$ and $C_4 = C_3 + C_2 + C_1$

$$\begin{aligned} &\Delta V_{k,i} = \Delta V_k^1 + \Delta V_k^2 + \Delta V_k^3 + \Delta V_k^4 \\ &\leq -\frac{v_{k-1} v_{k-1}}{2} - \eta\left|s_{k-1,i}\right|^{\frac{4}{3}} - \frac{4\alpha_3 \eta}{3} \int_{t_{0,k}}^{t} \left|s_{k,i}\right|^{\frac{4}{3}} d\tau \\ &-\alpha_3 \gamma \int_{t_{0,k}}^{t} s_{k,i} s_{k,i} d\tau - \frac{4}{3}\alpha_1 \eta \int_{t_{0,k}}^{t} \left|s_{k,i}\right| d\tau \\ &-\gamma \alpha_1 \int_{t_{0,k}}^{t} \left|s_{k-1,i}\right|^{\frac{5}{3}} d\tau - \gamma \frac{s_{k-1,i} s_{k-1,i}}{2} + C_4 \end{aligned} \tag{36}$$

Based on the Poincare map conclusion about ground impact error, $C_4 \in \mathbb{R}^-$. Therefore, 36 can be simplified as,

$$\begin{aligned} &\triangle V_k \leq -\frac{4\alpha_3 \eta}{3} \int_{t_{0,k}}^{t} \left|s_{k,i}\right|^{\frac{4}{3}} d\tau \\ &-\alpha_3 \gamma \int_{t_{0,k}}^{t} s_{k,i} s_{k,i} d\tau - \frac{4}{3}\alpha_1 \eta \int_{t_{0,k}}^{t} \left|s_{k,i}\right| d\tau, \end{aligned} \tag{37}$$

(37) is negative definite whenever $s_{k,i} \neq 0$ at least in one of the moments, $t \in [t_{0,k}, T]$. Therefore, it can be concluded that V_k is convergent. Because $V_k(t) \in \mathbb{R}^+$, This convergence ensures V_k converges to zero. Therefore, it ensures that the sliding surface and Ψwhich shows the estimation error of the system dynamics converge to zero. On the other hand, the dynamics of the sliding surface is Hurwitz. Hence, after this convergence, the output error is exponentially convergent to zero. To sum up, a second order ILCISM is designed to control system (17). In other word output y_i can be stabilized for $\forall i = 1...N-1$. It is robust with asymptotic stability to the system disturbance, allowing the system switches arbitrarily.

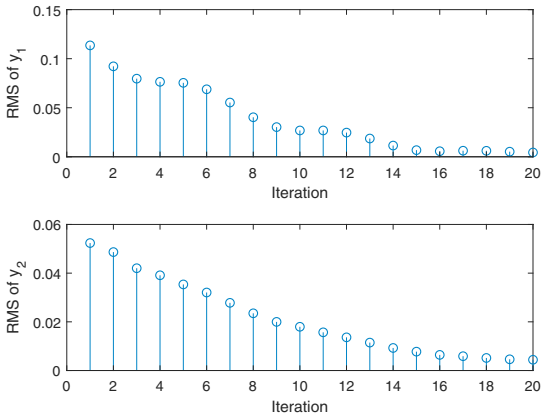

Fig. 2. Root mean square versus iterations

$V(s, e_0)$ given by (23) can be regarded as a common switched system Lyapunov function (9), hence, the stability result is consistent with the switching system theory [24].

C. Optimization Process

In the optimization process, the value of α_k^i in the Bezier polynomials in (13) should be chosen optimally in order to have a minimum effort movement. GAPSO and SQP combination method is used for the optimization. The global optimal convex region is found by GAPSO that satisfies the constraints and the absolute optimal solution is found by the SQP method in that region, which is found by GAPSO. For achieving minimum control effort, the following cost function is defined

$$J_{Eff} = \frac{1}{2p_2^h(q_0^-)} \int_0^{T_s} \sum_{i=1}^{m} (u_i(t))^2 dt, \tag{38}$$

where $u_i(t)$ is the control input, T_s is the step time, p_2^h is the length of a step, and m is the number of control inputs.

III. Simulation Results

The walking simulation is done for 100 seconds for $N = 3$. Fig. 2- 4 show the results, where a robust, optimal, and stable walking can be seen despite switching between the motor and FES as the muscle recovers or fatigues.

In Fig. 2, the root mean square (RMS) of the output tracking error is displayed during iterations of learning. As it can be seen it is reducing during different iterations. It shows that the learning term, σ_i is making system more robust in each iteration. The behavior of muscles fatigue is shown in Fig. (3) which is the switching main criterion. In the figure, S1-F and S1-S points show the stimulator 1 first and second switching respectively. S2-F and S2-S show the stimulator 2 first and second switching respectively. The angles and angular velocities of linkages are shown in Fig. (4). The abrupt angular velocities change, in Fig. (4), is because of the ground stride in each step. Note that the states are renominated after the double support phase which can be clearly seen in the figure.

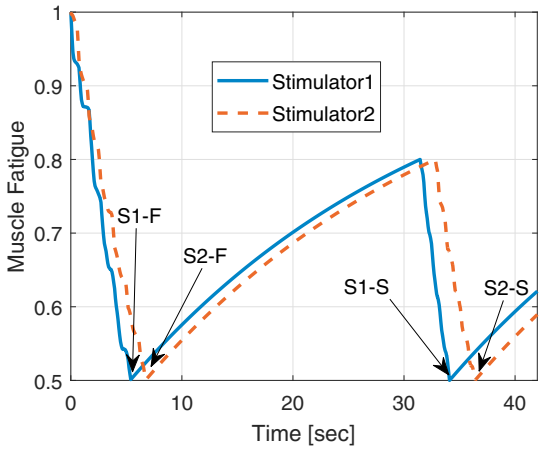

Fig. 3. Muscle fatigue behavior versus time

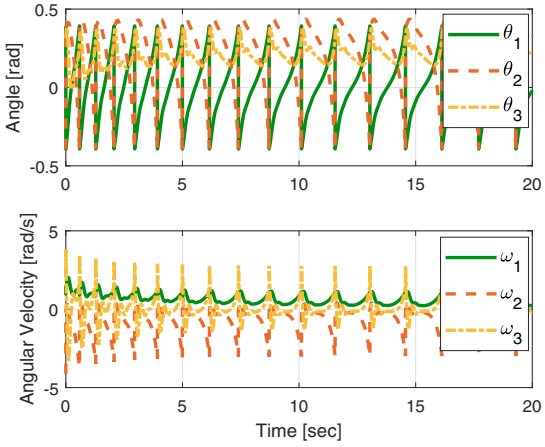

Fig. 4. Angle and angular velocities of the linkages versus time

IV. Conclusion

A switching controller that combines iterative learning and sliding mode control has been developed to coordinate FES and the powered exoskeleton. The sliding mode-based iterative learning control is used to learn the unknown functions in system dynamics. According to the simulated results, this technique helps the switching controller to decrease the RMS in each iteration. The controller stability was proven for using the Lyapunov-based stability analysis. The overall stability to account for impacts was shown numerically by using Poincare maps. The results exhibited the excellent performance of the proposed technique by-tracking the designed virtual constraints . Future work will be to experimentally test this technique on human subjects.

References

[1] A. del Ama, Á. Gil-Agudo, J. Pons, and J. Moreno, "Hybrid FES-robot cooperative control of ambulatory gait rehabilitation exoskeleton," *J. NeuroEng. Rehabil.*, vol. 11, no. 1, p. 27, 2014.

[2] K. Ha, S. Murray, and M. Goldfarb, "An approach for the cooperative control of FES with a powered exoskeleton during level walking for persons with paraplegia," *IEEE Trans. Neural Syst. Rehabil. Eng.*, 2015.

[3] N. Alibeji, N. Kirsch, and N. Sharma, "An adaptive low-dimensional control for a hybrid neuroprosthesis," in *IFAC*, vol. 48, pp. 303–308, Elsevier, 2015.

[4] H. Quintero, R. Farris, K. Ha, and M. Goldfarb, "Preliminary assessment of the efficacy of supplementing knee extension capability in a lower limb exoskeleton with FES," in *IEEE Eng. Med. Biol. Soc.*, no. 1, pp. 3360–3, 2012.

[5] N. A. Kirsch, X. Bao, N. A. Alibeji, B. E. Dicianno, and N. Sharma, "Model-based dynamic control allocation in a hybrid neuroprosthesis," *IEEE Transactions on Neural Systems and Rehabilitation Engineering*, vol. 26, pp. 224–232, Jan 2018.

[6] K. Ha, H. Quintero, R. Farris, and M. Goldfarb, "Enhancing stance phase propulsion during level walking by combining FES with a powered exoskeleton for persons with paraplegia," in *IEEE EMBC*, pp. 344–347, 2012.

[7] J. Contreras-Vidal, N. Bhagat, J. Brantley, J. Cruz-Garza, Y. He, Q. Manley, S. Nakagome, K. Nathan, S. Tan, and F. Zhu, "Powered exoskeletons for bipedal locomotion after spinal cord injury," *J. Neural Eng.*, vol. 13, no. 3, 2016.

[8] N. A. Alibeji, V. Molazadeh, B. E. Dicianno, and N. Sharma, "A control scheme that uses dynamic postural synergies to coordinate a hybrid walking neuroprosthesis: Theory and experiments," *Frontiers in Neuroscience*, vol. 12, p. 159, 2018.

[9] R. D. Gregg, T. Lenzi, N. P. Fey, L. J. Hargrove, and J. W. Sensinger, "Experimental effective shape control of a powered transfemoral prosthesis," in *2013 IEEE ICORR*, Jun 2013.

[10] H. Razavi, A. Bloch, X. Da, and A. Ijspeert, "Symmetric virtual constraints for periodic walking of legged robots," in *55st IEEE CDC*, Dec 2016.

[11] J. Grizzle, G. Abba, and F. Plestan, "Asymptotically stable walking for biped robots: analysis via systems with impulse effects," *IEEE Trans. Autom. Control*, vol. 46, no. 1, pp. 51–64, 2001.

[12] B. Griffin and J. Grizzle, "Nonholonomic virtual constraints for dynamic walking," in *54st IEEE CDC*, Dec 2015.

[13] N. Kirsch, N. Alibeji, B. E. Dicianno, and N. Sharma, "Switching control of functional electrical stimulation and motor assist for muscle fatigue compensation," in *ACC*, Jul 2016.

[14] E. R. Westervelt, J. W. Grizzle, C. Chevallereau, J. H. Choi, and B. Morris, *Feedback control of dynamic bipedal robot locomotion*, vol. 28. CRC press, 2007.

[15] R. D. Gregg and J. W. Sensinger, "Towards biomimetic virtual constraint control of a powered prosthetic leg," *IEEE Trans. Control Syst. Technol.*, vol. 22, pp. 246–254, Jan 2014.

[16] V. Molazadeh, Z. Sheng, and N. Sharma, "A within-stride switching controller for walking with virtual constraints: Application to a hybrid neuroprosthesis," in *ACC 2018*, IEEE, Accepted.

[17] Y. Hurmuzlu and D. B. Marghitu, "Rigid body collisions of planar kinematic chains with multiple contact points," *INT J ROBOT RES*, vol. 13, no. 1, pp. 82–92, 1994.

[18] E. R. Westervelt, J. W. Grizzle, and D. E. Koditschek, "Hybrid zero dynamics of planar biped walkers," *IEEE Trans. Autom. Control*, vol. 48, pp. 42–56, jan 2003.

[19] R. Riener and T. Fuhr, "Patient-driven control of FES-supported standing up: A simulation study," *IEEE Trans. Rehabil. Eng.*, vol. 6, pp. 113–124, 1998.

[20] R. Riener, J. Quintern, and G. Schmidt, "Biomechanical model of the human knee evaluated by neuromuscular stimulation," *J. Biomech.*, vol. 29, pp. 1157–1167, 1996.

[21] A. Isidori, *Nonlinear control systems*. Springer, 2013.

[22] Y. Shtessel, C. Edwards, L. Fridman, and A. Levant, *Sliding mode control and observation*. Springer, 2014.

[23] W. Chen, Y.-Q. Chen, and C.-P. Yeh, "Robust iterative learning control via continuous sliding-mode technique with validation on an srv02 rotary plant," *Mechatronics*, vol. 22, no. 5, pp. 588–593, 2012.

[24] D. Liberzon, *Switching in systems and control*. Springer, 2012.